

Article

The Influence of the Intramolecular 2D Interactions on the Physicochemical Properties of Hexasubstituted Benzene Derivatives

Agata Szlapa-Kula , Sławomir Kula , Patrycja Filipek , Stanisław Krompiec  and Michał Filapek 

Institute of Chemistry, Faculty of Science and Technology, University of Silesia in Katowice, Szkolna 9 St., 40-007 Katowice, Poland

* Correspondence: agata.szlapa-kula@us.edu.pl (A.S.-K.); michal.filapek@us.edu.pl (M.F.); Tel.: +48-32-359-1157 (M.F.)

Abstract: This paper contains a comprehensive study regarding the synthesis and physicochemical properties of new hexasubstituted benzene derivatives. In this work, three compounds of this type (including two electropolymerisable monomers) were synthesized in a one-step reaction with good yields ranging from 34% to 56%. A thermal investigation shows that this type of compound is stable up to 360 °C (10% weight loss temperature). The influence of the substituents in the first and second position of the central benzene on the stability, luminescence, and (spectro)electrochemical behavior was thoroughly studied with the aid of theoretical calculations. In each case, strong blue shifting of the π - π^* transition (according to 1,4-disubstituted analogs) was observed, proving this moieties' orthogonal orientation. In the case of derivatives with a Bt-core-Bt formula (where Bt = 2,2'-bithiophene-5-yl), an electrochemical oxidation process transformed them into conducting polymers. The polymer presents extraordinary stability during multiple p-doping; thus, spectroelectrochemical measurements of polymeric films were also performed.

Keywords: conducting polymers; cycloaddition; hexasubstituted benzene derivatives; optical properties; electrochemistry



Citation: Szlapa-Kula, A.; Kula, S.; Filipek, P.; Krompiec, S.; Filapek, M. The Influence of the Intramolecular 2D Interactions on the Physicochemical Properties of Hexasubstituted Benzene Derivatives. *Energies* **2023**, *16*, 480. <https://doi.org/10.3390/en16010480>

Academic Editor: Peter Foot

Received: 29 November 2022

Revised: 25 December 2022

Accepted: 27 December 2022

Published: 1 January 2023



Copyright: © 2023 by the authors. Licensee MDPI, Basel, Switzerland. This article is an open access article distributed under the terms and conditions of the Creative Commons Attribution (CC BY) license (<https://creativecommons.org/licenses/by/4.0/>).

1. Introduction

Hexasubstituted benzene (HSB) and its derivatives are used in many fields [1]. They can be used as anodes in organic photovoltaic cells [2], push-pull fluorophores [3], bioimaging derivatives [4], as a component in organic light-emitting diodes (OLED) [5] and in non-linear optics devices [6]. These applications result from the HSB derivatives physicochemical properties. While HSB derivatives were not studied much in the 20th century, we observed a significant increase in research reports on this topic over the past two decades. Contrary to the drawing formula, HSBs feature a remarkable non-planar structure in reality. This is due to the quickly rotating peripheral aromatic units concerning the central ring, which mimics the shape of a propeller [7]. However, this rotation is, in many cases, frozen. Almenningen et al. report a study of HSB electron diffraction in the gas phase and propose that the peripheral rings are positioned almost perpendicular to the central benzene [8]. Such an arrangement disfavors the intermolecular interactions (π - π and C-H \cdots π), while intramolecular 2D interactions are increased [9]. Consequently, this leads to higher HOMO values (the highest occupied molecular orbital) and LUMO (lowest molecular orbital gap) [10]. However, due to high intermolecular stabilization, they have attractive electronic, biological, and catalytic properties [11]. It is also worth noting that HSB derivatives exhibit many unique properties, such as aggregation induced emission efficiency. In addition, solvatochromism, with spectral shifts, a vast Stokes shift, and high thermal stability was observed for this type of compound. From a pure synthetic point of view, HSB shows easy accessibility and easy modification. The presence of various

structural variants allows for the developing of multiple types of fluorophores. Moreover, HSB has high solubility due to its 3D geometry [3,12]. As mentioned above, HSB exhibits exciting properties. Y. Liu and his group conducted a series of studies concerning HSB. The next step was to test the electrochemical properties by cyclic voltammetry, resulting in a reversible oxidative behavior, which affects high hole mobility [13].

HSB can also influence the HOMO energy level and the appropriate electron-donating or withdrawing groups. As a result, improved electron transport and emission behavior occurs. This makes HSB's potentially applicable in creating new types of electrical devices. These organic counterparts (which show high flexibility, viscosity, and low production cost) were able to replace the previous inorganic version [14]. Similar to hexaphenyl benzene, HSB finds various applications in organic light-emitting diodes and other photovoltaic applications. In addition, they have been used as organic dyes in dye photovoltaic cells [15]. HSBs can also be used in various electronic gadgets with low energy consumption and as organic field-effect transistors [16].

HSBs are also a type of derivative that can be used to study the TSCT (through-space charge transfer) process. This is due to their molecular architecture resulting from the company of six aromatic rings; as a result, the HSB has a propeller-like structure. On the other hand, this confirmation forces the aromatic units to face perpendicular to the central benzene ring (as mentioned before). This, in turn, causes an electronic interaction in the space between the aromatic substituents on the circumference. As a result, it can be observed that structures of this type exhibit thermally activated delayed fluorescence (TADF) and aggregation-induced emission (AIE) [17].

Additionally, HSB derivatives were tested by Y. Liu et al. for AIE. To evaluate the AIE feature, the series of the fluorescence spectra were measured and studied. With an increase in fw (water fraction) from 0% to 60%, an increase in fluorescence intensity was observed for two of the four compounds tested. However, when fw increased to 99%, a quenching and a redshift was observed, which could be caused by excimer emission or charge transfer emission for strong π - π interactions in the aggregated state [18].

HSBs play a significant role as they interact between distant redox-active units. This means that the redox-active site is on the fringes of the structure. They are attractive because of their high (potentially) stabilization properties; thus, they can participate in multi-stage redox processes through electron transport. Y. Tanaka carried out the synthesis of such HSBs, namely Hexa(phenyl) benzene and Hexa(thienyl) benzene complexes. Electrochemical measurements were then performed, which allowed for the analysis of symmetry and electrostatic repulsion. As a result of the study of these parameters, it was noticed that the three cationic centers were in meta positions to each other to avoid the phenomenon of electrostatic repulsion (this was the case with the first three oxidations). During the following three oxidation processes, the formation of cationic centers between the three already existing ones was observed. This shows that it is possible to modulate electrical communication in the case of HSB by changing the peripheral aromatic rings [19].

HSBs are an exciting type of molecule, but unfortunately, their preparation is often tricky. Xu Maotong et al. report the three-stage synthesis of hexasubstituted benzene using CO. The first step is to react the lithium complex $[(\text{Ph}_2\text{P}(\text{S}))_2\text{CLi}_2(\text{THF})_2]$ with carbon monoxide, forming a C-C bond and causing migration ($\text{Ph}_2\text{P}(\text{S})$). The next step is the oxidation of the previously obtained product with N_2O as a result of which oxidative cleavage of the P-C bond occurs. Finally, heating is carried out, causing cyclotrimerization. As a result, HSB free of transition metals is obtained [20]. As mentioned above, carrying out this type of reaction is quite troublesome, so Hui Zheng and his group wanted to optimize the synthesis of HSB. They focused on using DABCO (1,4-diazabicyclo[2.2.2]octane) as a promoting agent. The reaction itself is a domino reaction and consists of the reaction of arylidenemalononitrile with two molecules of dialkyl but-2-ynedionate. The sequence of the reaction is as follows: nucleophilic addition, Michael addition, annulation and, finally, aromatization. Simple reaction conditions are the main advantage of this type of reaction [21].

Trimerization, and especially cyclotrimerization supported by transition metal catalysts, attracts many chemists. This is because of its versatility in the synthesis of substituted aromatic compounds. The first example of cyclotrimerization was the nickel salt assisted cyclotrimerization of acetylene combined with phosphine ligands in the 1940s by Reppe. Since then, there has been substantial development in this field [22]. An alternative approach to transition metal catalyzed cyclotrimerization is currently to perform this cyclotrimerization under electrochemical conditions. K. Liang and his group performed a cobalt-catalyzed electrochemical cyclotrimerization of alkynes. The result was a six-membered ring under mild conditions and a controlled structure [23].

HSB can be obtained by the Diels-Alder reaction of tetraphenylcyclopentadienone derivatives and disubstituted alkynes [3]. It is worth noting that HSB can be further functionalized. Such functionalization may be by the Fields-Craft reaction. As a result of this reaction, precursors can be obtained that can play an essential role in nanographene synthesis [24].

Hexaarylbenzene is a good material for further functionalization. As a result, compounds with large structures with desirable properties can be obtained. An example of such a move is the obtaining of porphyrin conjugates. The synthesis of porphyrin with elongated pi bonds is of great interest because of its electrical and optical properties, which are obtained last, and, therefore, can be used, for example, in inorganic semiconductors. Porphyrin acts as a linker between hexaarylbenzenes that increases electrical communication. Ultimately, superbenzenoporphyrin conjugates (potential photosynthesis candidates) are obtained. The Scholl reaction can be used to get the desired effect. It is a reaction based on the formation of C-C bonds [25].

Techniques for expanding the π -electron structure and creating C-C bonds are still of interest due to the attractive properties of the compounds obtained. Reactions of this type are often selected to synthesize large scaffolds with extended π bonds. An example of such a reaction is the previously mentioned Scholl reaction [26]. The advantage of this reaction is the efficient growth of PAH (polycyclic aromatic hydrocarbon) and efficient synthesis. The Scholl reaction uses simple reagents, and they are Lewis acids or a combination of a Lewis or Brønsted acid and an oxidant AlCl_3 , MoCl_5 , or DDQ [27]. Another example of a reaction for HSB synthesis is the Diels-Alder [4 + 2] cycloaddition. This reaction is one of the most important reactions in modern synthesis. Combined with extrusion of CO or CO_2 , for example, followed by aromatization, the DA reaction allows obtaining products of various shapes and sizes [28]. This strategy allows the introduction into HSB structure moieties with desired properties [29,30].

2. Materials and Methods

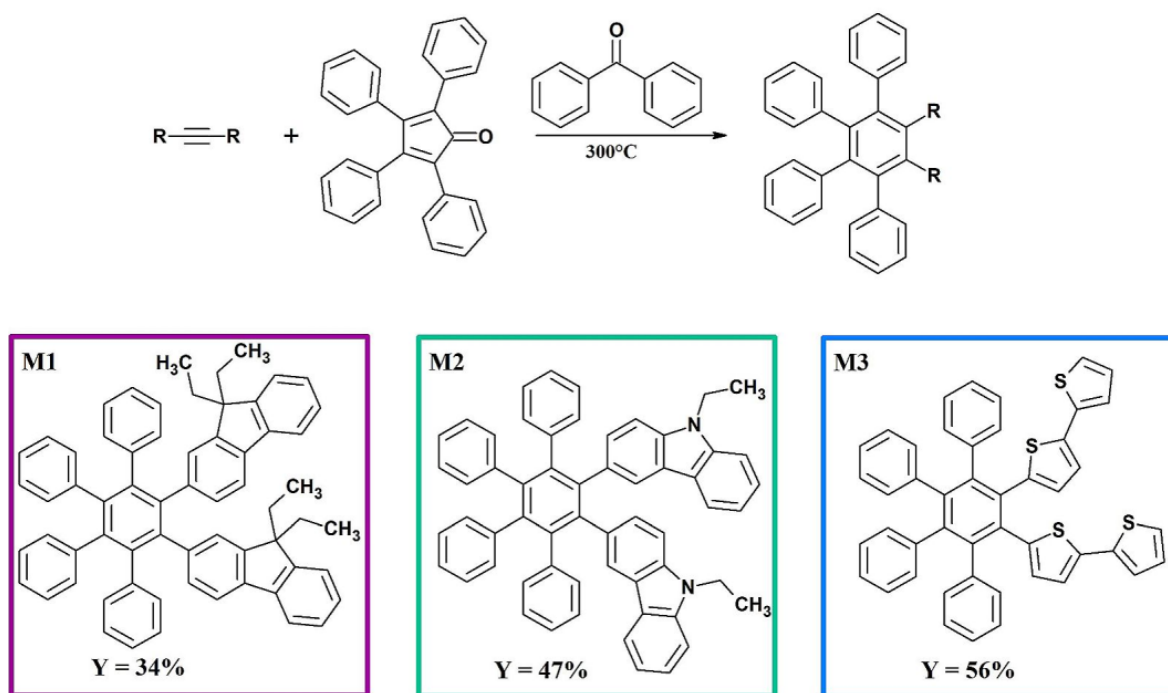
All information has been collected and placed in the Supporting Information (SI). Alkyne derivatives were obtained based on procedures described in the literature [31,32].

3. Results and Discussion

3.1. Synthesis and Characterization

The Diels-Alder [4 + 2] cycloaddition reactions have been intensively studied for many years. However, they still enjoy great interest and open up new paths in organic synthesis. An extremely interesting variant of this reaction is the Diels-Alder [4 + 2] cycloaddition between alkynes and a cyclopentadienone. Interestingly, it takes place in two stages. First, an intermediate cycloadduct is formed, from which the CO group then departs [33–35]. None of the steps require the use of a catalyst. All that is needed is a high temperature of 180 °C to 350 °C [36,37]. In the case of the tested compounds (M1–M3), they were obtained in the cycloaddition reaction (Diels-Alder [4 + 2]) of an appropriate alkyne with tetraphenylcyclopentadienone (Scheme 1). All reactions were carried out at a temperature of 300 °C under an argon atmosphere. The progress of the reaction was monitored by TLC chromatography. Benzophenone was used as a solvent. Excess tetraphenylcyclopentadienone and benzophenone were easily disposed of by column

chromatography. As a result of the conducted reactions, three hexasubstituted benzene derivatives (**M1–M3**) were obtained, with the yields in the range of 34–56%.



Scheme 1. Synthesis and structures of hexasubstituted benzene derivatives (**M1–M3**).

3.2. Thermal Properties

Research on the thermal stability of chemical compounds is fundamental in determining the possibility of their use. Therefore, the **M1–M3** derivatives were tested by thermogravimetric analysis (Figure 1 and Table 1). Interestingly, the tested compounds differ in thermal properties. The derivative **M3** is the least stable. Its 5% weight loss (T_5) is already observed at 343°C . On the other hand, the replacement of 2,2'-bithiophene-5-yl substituents with N-ethyl-9H-carbazol-3-yl increases **M3** stability (by 57°C) to 400°C . The best results are characterized by **M1** ($T_5 = 437^\circ\text{C}$) having two 9,9-diethyl-9H-fluoren-2-yl substituents. Considering the obtained results, we can assume that the two substituents 2,2'-bithiophene-5-yl in the **M3** structure (in ortho positions related to each other) undergo partial thermal destruction at the temperature of 343°C .

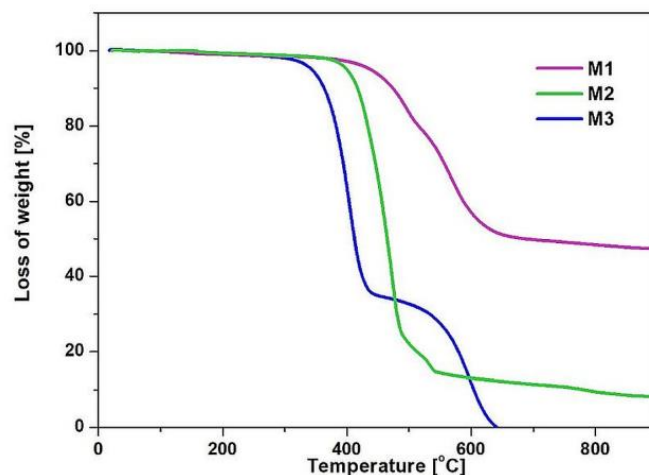


Figure 1. Thermal properties of **M1–M3**.

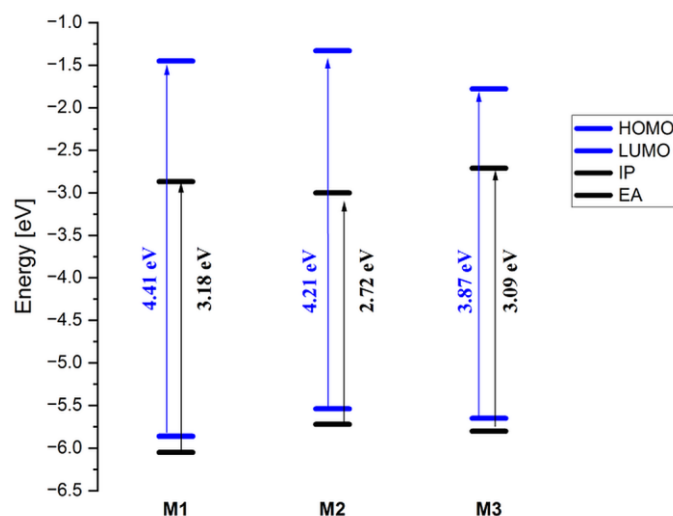
Table 1. Thermal stability of M1–M3.

Code	T ₅ ¹ [°C]	T ₁₀ ¹ [°C]	T _{max} ² [°C]
M1	437	473	495; 571
M2	400	417	469
M3	343	363	404; 596

¹ T₅ and T₁₀ are the temperature at 5% and 10% weight loss, respectively. ² T_{max} is the temperature of maximum decomposition rate.

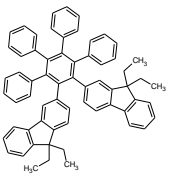
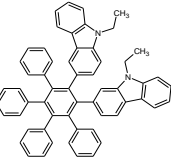
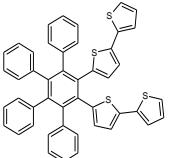
3.3. DFT Calculations

DFT calculations are a helpful tool for explaining phenomena and properties in research. Therefore, to better understand the influence of the substituents of the presented molecules on the physicochemical properties, DFT and TD-DFT calculations were performed. The calculations were made with the Gaussian 16 program [38]. In the first step for the selected derivative M3, optimization of the molecular geometry was performed in three different various exchange-correlation functionals with the bases B3LYP/6-311+G** [39], CAM-B3LYP/6-311+G** [40] and PBE1PBE/def2TZVP [41–43] (see Figure S1 in SI). The shape and position of the HOMO and LUMO orbitals are presented in Table S1 (in SI). Based on the obtained geometry, TD-DFT calculations were performed. All calculations were performed in dichloromethane. The results of the calculations showed that B3LYP/6-311+G** is the best base due to the degree of matching the calculations to the experimental values. Therefore, B3LYP/6-311+G** was used to calculate the rest of the compounds. It is worth noting that in each case, substituents in the first and second positions are orthogonal (relative to the core ring), which is in agreement with geometries calculated for the similar compounds [44]. HOMO orbitals for the analyzed benzene derivatives (M1–M3) are located on π -excess substituents, which are 2,2'-bithiophene-5-yl, 9,9-diethyl-9H-fluoren-2-yl or N-ethyl-9H-carbazol-3-yl fragments. The calculated energy values of the HOMO orbitals for all molecules (−5.86 eV for M1, −5.54 eV for M2, −5.65 eV for M3) agree with the experimental data (Figure 2). For compound M1, the energy value of the HOMO orbital is the lowest and amounts to −5.86 eV. In turn, the LUMO orbitals for the M1, M2 and M3 derivative include anti-binding orbitals of the phenyl ring being the core of the molecules and the orbitals of the 2,2'-bithiophene-5-yl, 9,9-diethyl-9H-fluoren-2-yl or N-ethyl-9H-carbazol-3-yl systems. Interestingly, for the M3 derivative, the LUMO orbital has the lowest energy value (−1.78 eV), which would suggest that this compound will undergo the reduction process most easily.

**Figure 2.** Molecular orbital energy level graph of M1–M3.

As can be seen (Figure 2), the energy gap values for derivatives **M1–M3** are different. We observe a decreasing trend in the magnitude of the energy gap by approximately 0.2–0.3 eV. Compound **M3** shows the smallest energy gap, which is mainly due to the low LUMO energy value. The HOMO energy value for **M2** (as in the case of **M3**) suggests that this compound will easily undergo oxidation, although the reduction process will not be as favorable as for **M3**, increasing the energy gap by about 0.3 eV. For the compound **M1**, both processes will be difficult; therefore, the E_g of this molecule will be the largest. The DFT calculations performed were consistent with the results obtained experimentally for all molecules under consideration. Based on the obtained geometry, TD-DFT calculations were then performed. The experimental and theoretical spectra are presented in Table 2. All compounds absorb light in a wide band with an absorption maximum between 337 nm and 409 nm. The first band describes the π - π^* transitions. This band corresponds to the HOMO \rightarrow LUMO transitions. In the case of the **M2** compound in the discussed band, we are also dealing with H-1 \rightarrow LUMO and HOMO \rightarrow L + 1 transitions. The oscillator strength for all transitions corresponds to HOMO \rightarrow LUMO above 0.04.

Table 2. Redox potentials, HOMO and LUMO energies and electrochemical band gaps (E_g).

Code	E_{1red} [V]	E_{1ox} [V]	E_{2ox} [V]	HOMO ¹ (CV)	LUMO ² (CV)	$E_g(CV)$ ³ [eV]	λ_{onset} [nm]	$E_{g(opt)}$ ⁴	HOMO (DFT)	LUMO (DFT)	$E_{g(DFT)}$ [eV]	
	M1	−2.23	0.95						−5.86	−1.45	4.41	
	M2	−2.1	0.62	0.81	−5.72	−3.00	2.72	366	3.39	−5.54	−1.33	4.21
	M3	−2.39	0.7		−5.8	−2.71	3.09	480	2.58	−5.65	−1.78	3.87

¹ HOMO = $-5.1 - E_{ox}$; ² LUMO = $-5.1 - E_{red}$; ³ $E_g = E_{ox}(onset) - E_{red}(onset)$; ⁴ $1240/\lambda_{onset}$.

3.4. Optical Characterization

The photophysical properties of investigated compounds were evaluated by UV-vis and photoluminescence (PL) measurements in diluted solutions.

As shown in Figure 3, all of the investigated compounds absorb light in the high-energetic visible region—i.e., between 320 nm and 475 nm. As is well known, most of the derivatives bearing carbazole or bithienyl moieties are generally colored; thus they absorb light with longer wavelengths. In the case of compounds investigated within this paper, we observed strong blue-shifting of the π - π^* transitions ascribed to heteroaromatic electrons. This is the direct consequence of the orthogonal orientation of the substituents and the central phenyl moiety that prevent resonance contact. It is worth noting that the excitation spectra exhibit several peak maxima for each investigated compound. In the case of **M1** in the 200–800 nm region, the excitation spectrum exhibit two maxima: at 274 nm and 362 nm, yielding (for both wavelengths) emission with the maximum of 431 nm (i.e., giving Stokes shifts as high as 157 nm and 69 nm, respectively). It is a well-known fact that the high values of the Stokes shift are caused by intermolecular charge transfer (ICT). The difference in the above-mentioned values suggests that the first of the transitions are ICT processes, while the second one occurs within the same molecule

fragment (which was confirmed by DFT calculation). For **M2**, the obtained spectra are even more complex. As one can see in Figure 4C, the excitation spectra exhibit 4 maxima at 332 nm, 350 nm, 270 nm and 405 nm. When the emission spectra for excitation in those wavelengths were measured, we observed that in each case the result spectrum with two maxima was recorded. However, the two highest energetic light peaks with a maximum at 388 nm dominates, while for two others (i.e., excitation = 370 nm and 405 nm), another peak dominates, with a maximum at 465 nm. This behavior suggests that the HOMO orbital lies at a large area of the molecule, and after excitation, a charge is distributed and then emission takes place from two different parts of the molecule. The **M3** spectrum also consists of several transitions. Thus, for this compound, experiments with different excitation wavelengths were conducted. Excitation by light with $\lambda_{\text{ex}} = 285$ nm gives the broad emission spectrum with peak maximum = 388 nm. On the other hand, $\lambda_{\text{ex}} = 394$ nm and $\lambda_{\text{ex}} = 465$ nm force the compound to emit light with a peak maximum = 478 nm and 524 nm, respectively.

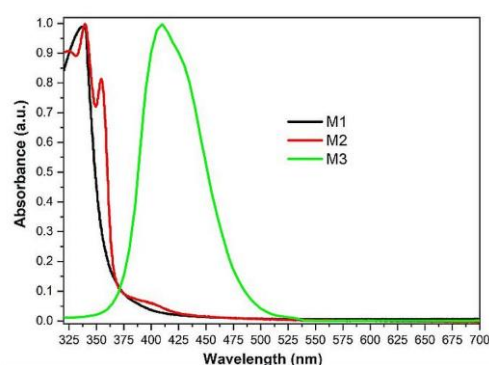


Figure 3. UV-vis absorption spectra of investigated compounds: in CH_2Cl_2 ($c = 1 \times 10^{-5}$ M).

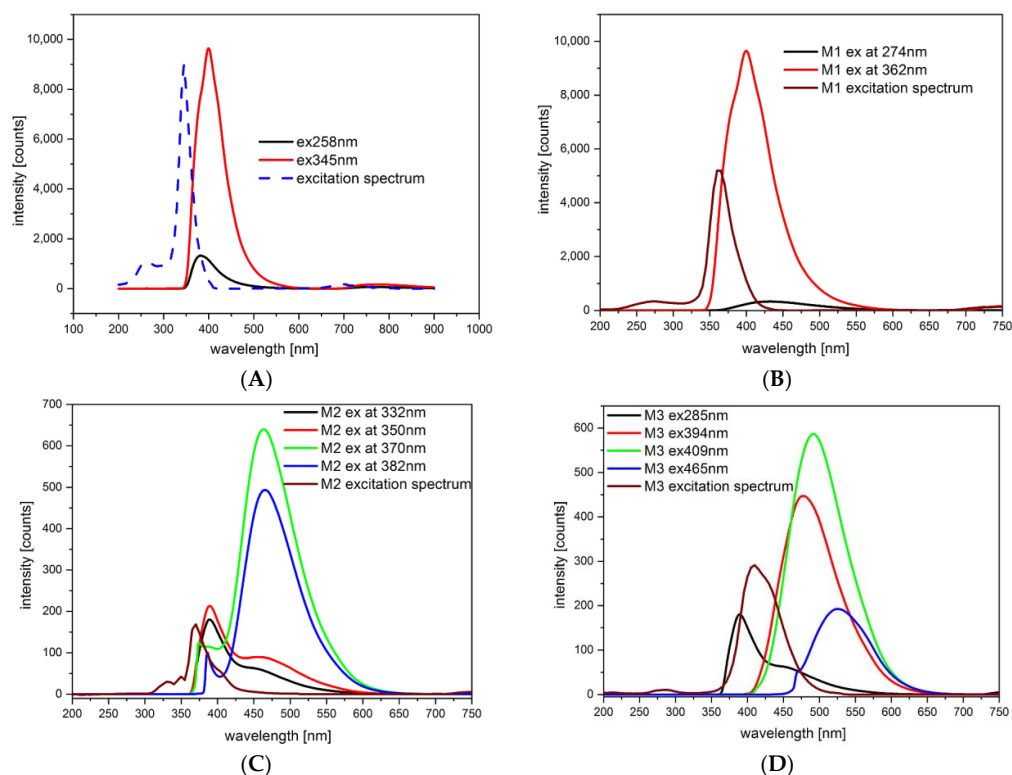


Figure 4. Emission and excitation spectra of investigated compounds: (A) **M1** in MeCN ($c = 1 \times 10^{-5}$ M); (B) **M1** in CH_2Cl_2 ($c = 1 \times 10^{-5}$ M); (C) **M2** in CH_2Cl_2 ($c = 1 \times 10^{-5}$ M); (D) **M3** in CH_2Cl_2 ($c = 1 \times 10^{-5}$ M).

3.5. Electrochemical Characterization

All of the obtained compounds were investigated electrochemically in their diluted CH_2Cl_2 solutions. By using cyclic voltammetry (CV), one can easily estimate a molecule's HOMO and LUMO energy level and energy gap (Eg), assuming the IP of ferrocene equals -5.1 eV [45].

First, the electrochemical properties during negative potential sweeping were investigated. As can be seen in Figure 5, in each cases' reduction (X/X^- process), the peak onset is as follows: -2.23 V, -2.1 V and -2.39 V, so it is relatively difficult compared with similar fluorene, carbazole or bithiophene derivatives, respectively. This suggests an existing strong 2D-resonance between six substituents of the central phenyl core. In the neutral form, the wire current in each of the above-mentioned moieties interacts magnetically with neighboring aromatic rings, which stiffens the molecule and lowers the energy. After reduction, the aforementioned interaction is forbidden. Moreover, additional electron density should cause the repulsion of the substituents. Another confirmation of the existence of 2D-interactions was found during investigations of the compounds during positive potential sweeping. In this case, the potential needed for oxidation (X/X^+ process) is lowered. This is the direct consequence of the electronic interaction of the moieties in ortho positions to each other, the stabilizing carbocation being "produced" during oxidation. It is worthy of note that compound **M2** from the formal point of view is an electropolymerizable monomer (i.e., it poses two terminal carbazole moieties), but stabilization is so high that even the second oxidation step is reversible (see Figure 5). Only in the case of **M3**, during the positive potential sweep (Figure 6), was the polythiophene film at the electrode surface deposited. Deposited polythiophenes were examined in monomer-free solution proving their stability during both n- and p-doping (Figures 7 and 8) [46–48].

In the next step, a series of spectroelectrochemical experiments with external potential slightly above oxidation potential were conducted. In the case of compound **M3**, oxidation is an irreversible process, causing the electropolymerization of the specie.

In the first stage of the oxidation process, an additional band appears and grows in the 400–500 nm range (see Figure 9). At this potential, the monomer dimerization leads to the formation of the quaterthiophene bridges. Moreover, the polaronic band [49,50] is also observed (it is, however, of low intensity). On the other hand, when the external potential is raised to 1.1 V, more visible changes occur, and the spectrum becomes characteristic for the doped polymer [51–53]. As expected, when the external potential is restored to 0V, the appearance of the spectrum does not return to its original appearance, but an additional band (within 400 and 500 nm) is maintained. It is worthy of note that the polaronic band disappears completely. Next, as a comparison, the electropolymerization on the ITO electrode (potentiodynamically) with an upper potential as high as 0.82 V was also carried out. The resulting polymer was then also investigated spectroelectrochemically in a monomer-free solution. After applying the potential as high as 1.1 V, the polymer behaves very similarly to the one obtained by the potentiostatic method. The main difference is that no evident maxima can be observed in this case, suggesting that the potentiodynamic route enforces a higher distribution of chain lengths or dimerization via the third or fourth positions of the terminal thiophene rings. Moreover, in the case of conjugated monomers, electropolymerization using the potentiodynamic route lead to materials containing short-chain oligomers [54].

As was already mentioned, the compound **M2** undergoes two-step reversible oxidation, which is uncommon for compounds with a carbazole moiety [55,56]. During a spectroelectrochemical experiment using an external potential as high as 0.7V, new bands with maximum wavelengths at 410 nm and 1050 appear (Figure 10). Considering the case of electrochemical measurements in solution, the rate of generation of the oxidized species could be low. Thus, the above-mentioned potential was held to increase the product's concentration. As one can see, this experiment band with a maximum of 410 nm become well defined and sharp.

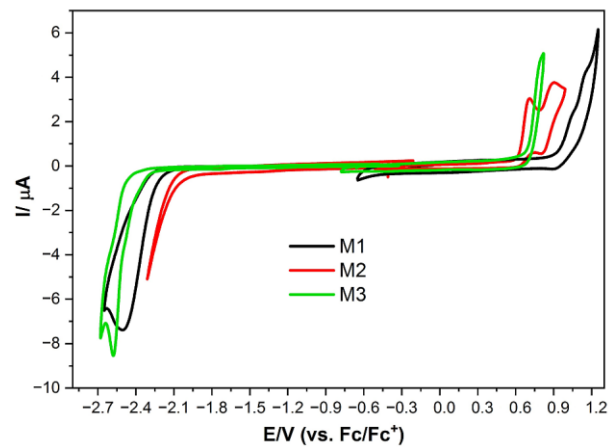


Figure 5. Voltammograms of the investigated compounds; sweep rate $\nu = 100$ mV/s, 0.1 M Bu_4NPF_6 in CH_2Cl_2 .

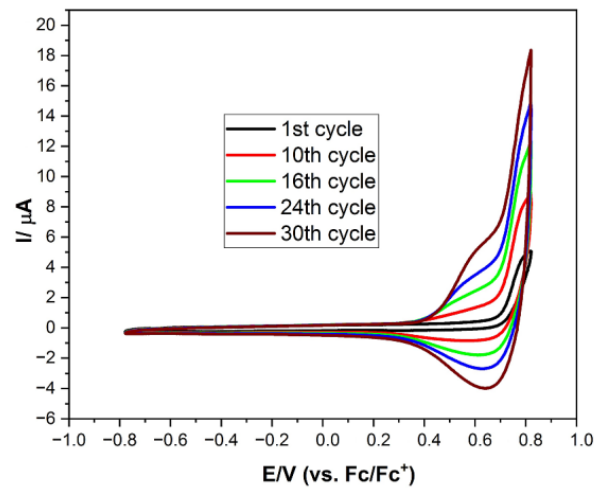


Figure 6. Voltammograms of polymerization of M3 carried out potentiodynamically with upper potential as high as 0.82 V, with sweep rate $\nu = 100$ mV/s, 0.1 M Bu_4NPF_6 in CH_2Cl_2 .

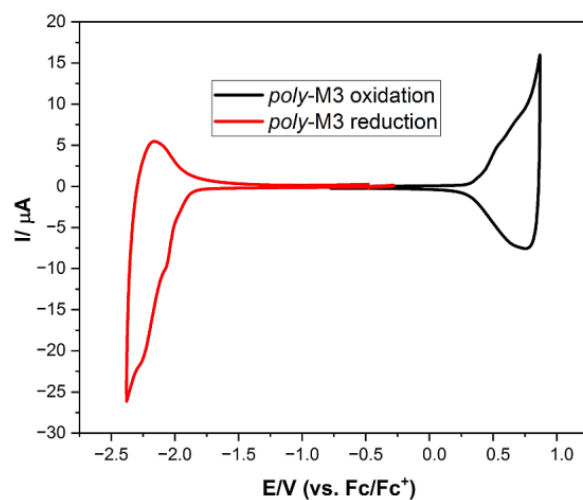


Figure 7. Voltammograms of *poly-M3* (polymerization carried out potentiodynamically with upper potential as high as 0.82 V) with sweep rate $\nu = 100$ mV/s, 0.1 M Bu_4NPF_6 in CH_2Cl_2 .

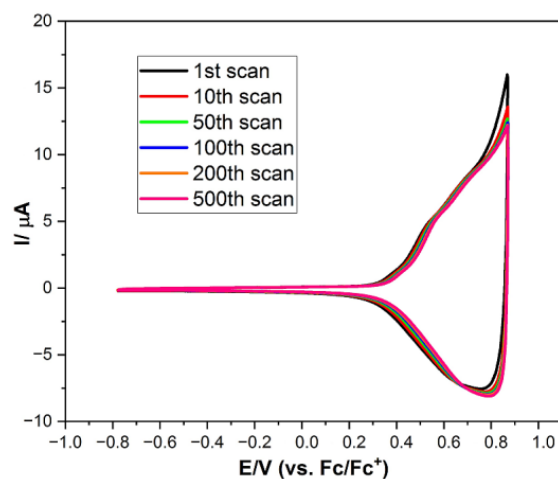


Figure 8. Voltammograms of *poly-M3* (polymerization carried out potentiodynamically with upper potential as high as 0.82 V) with sweep rate $\nu = 100$ mV/s, 0.1 M Bu_4NPF_6 in CH_2Cl_2 . Only some of the obtained cycles are presented (for clarity).

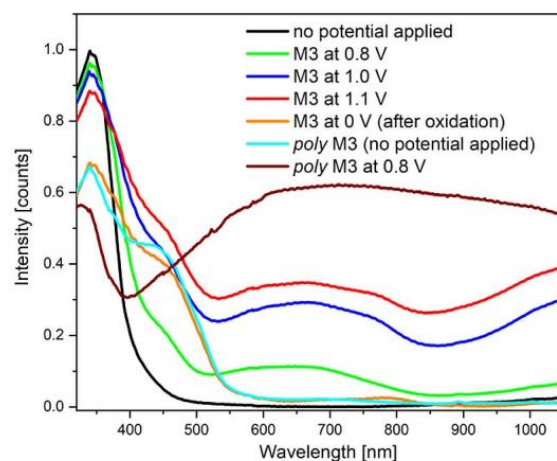


Figure 9. UV-Vis spectroelectrochemistry of the **M3** derivative in chloroform solution ($c = 1 \times 10^{-4}$ mol/L, as an inset on the graph potentials vs. Fc/Fc^+ redox couple).

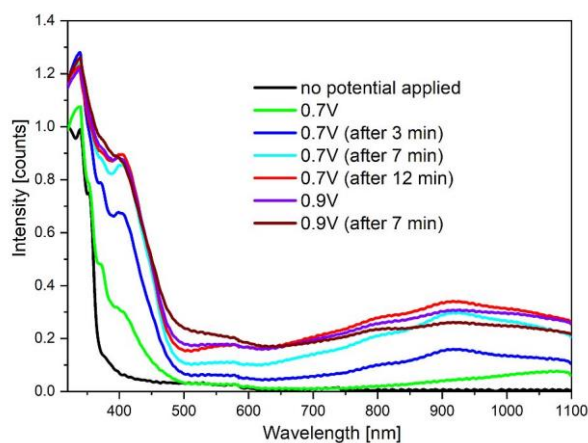


Figure 10. UV-Vis spectroelectrochemistry of the **M2** derivative in chloroform solution ($c = 1 \times 10^{-4}$ mol/L, as an inset on the graph potentials vs. Fc/Fc^+ redox couple).

On the other hand, a broad band covering the whole spectrum also increases its absorbance value. This type of spectrum is characteristic of species possessing a long chain of the conjugated double bond. In the next step, the potential was shifted and held at a value above E_{2ox} (i.e., to potential allowing conversion of the compound into dication). Under these conditions, the magnitude of the band laying between 600 nm and 1100 nm is lowered slightly, while the band between 480 nm and 600 nm is increased.

4. Conclusions

This paper was devoted to the synthesis of the hexasubstituted phenyl derivatives. All compounds were synthesized in a one-step reaction with good yields. It was proven that all molecules are thermally stable up to 340 °C. All compounds absorb light in a wide band with an absorption maximum between 337 nm and 409 nm. The first band is ascribed to the π - π^* transitions which correspond to the HOMO \rightarrow LUMO transitions. The results of the calculations showed that B3LYP/6-311+G** is the best basis due to the degree of matching the calculations to the experimental values (for this type of molecule). Optimized geometry shows that in each case, the substituents in the first and second positions are orthogonal (relative to the core ring), affecting strong intramolecular 2D interactions. An electrochemical investigation revealed that reduction limits the above-mentioned interaction; thus, reduction (X/X $^-$ process) is relatively hampered in each case. On the other hand, the potential needed for oxidation (X/X $^+$ process) is lowered. This is the direct consequence of the electronic interaction of the moieties in ortho positions to each other, stabilizing carbocation "produced" during oxidation. A compound possessing two terminal carbazole moieties is a formally electropolymerizable monomer, but 2D stabilization is so high that even the second oxidation step is reversible. During spectroelectrochemical measurements (above E_{ox}), broadband covering the whole spectrum was created. This spectrum type is characteristic for the species possessing a long chain of the conjugated double bond. In the case of an analog with bithienyl moieties, polythiophene film was deposited at the electrode surface during oxidation. A spectroelectrochemical investigation confirmed the formation of a polaronic band during p-doping. The above-mentioned polymer is the first example of the electrochemically obtained conductive polymer with a hexasubstituted benzene core in the main chain.

Supplementary Materials: The following supporting information can be downloaded at: <https://www.mdpi.com/article/10.3390/en16010480/s1>, Figure S1: Experimental (gray line) absorption spectra and calculated transitions of **M3** in dichloromethane at B3LYP/6-311+G**, CAM-B3LYP/6-311+G** and PBE1PBE/def2TZVP; Table S1: The HOMO and LUMO levels; Table S2: The energies and characters of the selected spin-allowed electronic transitions for **M1**, **M2** and **M3** calculated with the B3LYP/6-311+G** method, together with assignment to the experimental absorption bands; Table S3: The energies and characters of the selected spin-allowed electronic transitions for **M1**, **M2** and **M3** calculated with the B3LYP/6-311+G** method, together with assignment to the experimental absorption bands; Figure S2: Experimental (blue line) absorption spectra and calculated transitions (black) of **M1–M3** in dichloromethane (at B3LYP/6-311+G level); Figure S3: ^1H NMR of **M3**; Figure S4: H-H COSY of **M3**; Figure S5: ^{13}C NMR of **M3**; Figure S6: H-C HMQC of **M3**; Figure S7: H-C HMBC of **M3**.

Author Contributions: Conceptualization, A.S.-K. and M.F.; methodology, A.S.-K., S.K. (Sławomir Kula) and M.F.; validation, S.K. (Sławomir Kula), A.S.-K. and M.F.; formal analysis, S.K. (Sławomir Kula), P.F., S.K. (Stanisław Krompiec), A.S.-K. and M.F.; investigation, S.K. (Stanisław Krompiec), P.F., S.K. (Sławomir Kula), A.S.-K. and M.F.; resources, S.K. (Stanisław Krompiec); data curation, P.F.; writing—original draft preparation, A.S.-K., S.K. (Sławomir Kula) and M.F.; writing—review and editing, A.S.-K. and M.F.; visualization, A.S.-K. and M.F.; supervision, A.S.-K. and M.F.; project administration, A.S.-K. and M.F.; funding acquisition, S.K. (Stanisław Krompiec). All authors have read and agreed to the published version of the manuscript.

Funding: This research was funded by National Science Centre of Poland, grant numbers 2017/01/X/ST5/01786 and 2019/33/B/ST4/00962.

Data Availability Statement: Not applicable.

Acknowledgments: Calculations have been carried out using resources provided by Wrocław Centre for Networking and Supercomputing (<http://wcss.pl>, accessed on 11 November 2021), grant No. 18.

Conflicts of Interest: The authors declare that they have no conflicts of interest.

References

1. Kumar, A.; Yadav, M.K.; Singh, J.; Singh, J.D.; Butcher, R.J. Facile synthesis of mixed O, S or Se bearing hexasubstituted benzenes and their potential as Cu (II) ion probe. *Dalton Trans.* **2019**, *48*, 5627–5636. [[CrossRef](#)] [[PubMed](#)]
2. Stuzhin, P.A.; Skvortsov, I.A.; Zhabanov, Y.A.; Somov, N.V.; Razgonyaev, O.V.; Nikitin, I.A.; Koifman, O.I. Subphthalocyanine azaanalogues–Boron (III) subporphyrazines with fused pyrazine fragments. *Dyes Pigment.* **2019**, *162*, 888–897. [[CrossRef](#)]
3. Yin, G.; Li, Y.; Li, S.; Xu, B.; Yang, Q.; Zhang, Y.; Zhao, J.; Cao, X. Hexaphenylbenzene based push-pull fluorophores displaying intriguing polarity-dependent fluorescence behavior, AIE(E) characteristics and mega-large Stokes shifts. *Dyes Pigment.* **2022**, *198*, 110013. [[CrossRef](#)]
4. Wang, S.; Li, B.; Zhang, F. Molecular fluorophores for deep-tissue bioimaging. *ACS Cent. Sci.* **2020**, *6*, 1302–1316. [[CrossRef](#)]
5. Teng, J.M.; Wang, Y.F.; Chen, C.F. Recent progress of narrowband TADF emitters and their applications in OLEDs. *J. Mater. Chem. C* **2020**, *8*, 11340–11353. [[CrossRef](#)]
6. Wu, J.; Luo, J.; Jen, A.K.Y. High-performance organic second-and third-order non-linear optical materials for ultrafast information processing. *J. Mater. Chem. C* **2020**, *8*, 15009–15026. [[CrossRef](#)]
7. Vij, V.; Bhalla, V.; Kumar, M. Hexaarylbenzene: Evolution of properties and applications of multitiered scaffold. *Chem. Rev.* **2016**, *116*, 9565–9627. [[CrossRef](#)]
8. Almenningen, A.; Bastiansen, O.; Skancke, P.N. Electron diffraction studies of hexaphenylbenzene vapour. *Acta Chem. Scand.* **1958**, *12*, 1215–1220. [[CrossRef](#)]
9. Gagnon, E.; Maris, T.; Arseneault, P.M.; Maly, K.E.; Wuest, J.D. Structural features in crystals of derivatives of benzene with multiple contiguous phenyl substituents. *Cryst. Growth Des.* **2010**, *10*, 648–657. [[CrossRef](#)]
10. Gagnon, E.; Halperin, S.D.; Metivaud, V.; Maly, K.E.; Wuest, J.D. Tampering with molecular cohesion in crystals of hexaphenylbenzenes. *J. Org. Chem.* **2010**, *75*, 399–406. [[CrossRef](#)]
11. Kwon, S.M.; Won, J.K.; Jo, J.W.; Kim, J.; Kim, H.J.; Kwon, H.I.; Park, S.K. High-performance and scalable metal-chalcogenide semiconductors and devices via chalcogen-gel routes. *Sci. Adv.* **2018**, *4*, eaap910. [[CrossRef](#)] [[PubMed](#)]
12. Popczyk, A.; Cheret, Y.; El-Ghayoury, A.; Sahrhoui, B.; Mysliwiec, J. Solvatochromic fluorophores based on thiophene derivatives for highly-precise water, alcohols and dangerous ions detection. *Dyes Pigment.* **2020**, *177*, 108300. [[CrossRef](#)]
13. Liu, Y.; Tao, C.; Xie, G.; Van Der Velden, J.; Marras, S.; Luo, Z.; Yang, C. Hexa-substituted benzene derivatives as hole transporting materials for efficient perovskite solar cells. *Dyes Pigment.* **2019**, *163*, 267–273. [[CrossRef](#)]
14. Devibala, P.; Balambiga, B.; Noureen, S.; Nagarajan, S. Hexaarylbenzene based high-performance p-channel molecules for electronic applications. *RSC Adv.* **2021**, *11*, 11672–11701. [[CrossRef](#)]
15. Krzeszewski, M.; Thorsted, B.; Brewer, J.; Gryko, D.T. Tetraaryl-, pentaaryl-, and hexaaryl-1, 4-dihydropyrrolo [3, 2-b] pyrroles: Synthesis and optical properties. *J. Org. Chem.* **2014**, *79*, 3119–3128. [[CrossRef](#)]
16. Jhulki, S.; Moorthy, J.N. Small molecular hole-transporting materials (HTMs) in organic light-emitting diodes (OLEDs): Structural diversity and classification. *J. Mater. Chem. C* **2018**, *6*, 8280–8325. [[CrossRef](#)]
17. Wang, X.; Wang, S.; Lv, J.; Shao, S.; Wang, L.; Jing, X.; Wang, F. Through-space charge transfer hexaarylbenzene dendrimers with thermally activated delayed fluorescence and aggregation-induced emission for efficient solution-processed OLEDs. *Chem. Sci.* **2019**, *10*, 2915–2923. [[CrossRef](#)]
18. Liu, Y.; Mao, X.; Wang, X.; Bai, J.; Zhang, J.; Feng, X.; Yamato, T. Pyrene-based asymmetric hexaarylbenzene derivatives: Synthesis, crystal structures, and photophysical properties. *J. Lumin.* **2022**, *243*, 118653. [[CrossRef](#)]
19. Tanaka, Y.; Akita, M. Synthesis and intramolecular electronic interactions of hexaarylbenzene bearing redox-active Cp*(dppe) Fe-C≡C-termini. *J. Organomet. Chem.* **2018**, *878*, 30–37. [[CrossRef](#)]
20. Xu, M.; Wang, T.; Qu, Z.W.; Grimme, S.; Stephan, D.W. Reactions of a Dilithiomethane with CO and N₂O: An Avenue to an Anionic Ketene and a Hexafunctionalized Benzene. *Angew. Chem.* **2021**, *133*, 25485–25489. [[CrossRef](#)]
21. Zheng, H.; Han, Y.; Sun, J.; Yan, C.G. Convenient synthesis of hexasubstituted benzene derivatives via DABCO promoted domino reaction of arylidene malononitrile and dialkyl but-2-ynedioate. *Chin. Chem. Lett.* **2021**, *32*, 1683–1686. [[CrossRef](#)]
22. Yamamoto, K.; Nagae, H.; Tsurugi, H.; Mashima, K. Mechanistic understanding of alkyne cyclotrimerization on mononuclear and dinuclear scaffolds: [4 + 2] cycloaddition of the third alkyne onto metallacyclopentadienes and dimetallacyclopentadienes. *Dalton Trans.* **2016**, *45*, 17072–17081. [[CrossRef](#)] [[PubMed](#)]
23. Liang, K.; Lu, L.; Liu, X.; Yang, D.; Wang, S.; Gao, Y.; Lei, A. Electrochemical Cobalt-catalyzed Cyclotrimerization of Alkynes to 1, 2, 4-Substituted Arenes. *ACS Catalysis* **2021**, *11*, 14892–14897. [[CrossRef](#)]
24. Johnson, M.A.; Martin, M.; Cocq, K.; Ferguson, M.; Jux, N.; Tykwinski, R.R. Acylation of Hexaphenylbenzene for the Synthesis of [5]Cumulenes. *Eur. J. Org. Chem.* **2022**, *2022*, e202101467. [[CrossRef](#)]
25. Nisa, K.; Khatri, V.; Kumar, S.; Arora, S.; Ahmad, S.; Dandia, A.; Chauhan, S.M. Synthesis and redox properties of superbenzene porphyrin conjugates. *Inorg. Chem.* **2020**, *59*, 16168–16177. [[CrossRef](#)]

26. Jassas, R.S.; Mughal, E.U.; Sadiq, A.; Alsantali, R.I.; Al-Rooqi, M.M.; Naeem, N.; Ahmed, S.A. Scholl reaction as a powerful tool for the synthesis of nanographenes: A systematic review. *RSC Adv.* **2021**, *11*, 32158–32202. [[CrossRef](#)]
27. Ponugoti, N.; Venkatakrishnan, P. Rearrangements in Scholl Reaction. *Chem. Eur. J.* **2021**, *28*, e202103530. [[CrossRef](#)]
28. Krompiec, S.; Kurpanik-Wójcik, A.; Matussek, M.; Gofek, B.; Mieszczanin, A.; Fijolek, A. Diels–Alder Cycloaddition with CO, CO₂, SO₂, or N₂ Extrusion: A Powerful Tool for Material Chemistry. *Materials* **2021**, *15*, 172. [[CrossRef](#)]
29. Zhang, Y.; Guo, J.; Li, X.; Zhao, M.; Wei, Q.; Song, P. One- and two-photon absorption properties of quadrupolar A– π –D– π –A dyes with donors of varying strengths. *Spectrochim. Acta A* **2020**, *230*, 118015. [[CrossRef](#)]
30. Wang, H.; Wang, P.; Niu, L.; Liu, C.; Xiao, Y.; Tang, Y.; Chen, Y. Carbazole-thiophene based fluorescent probe for selective detection of Cu²⁺ and its live cell imaging. *Spectrochim. Acta A* **2022**, *278*, 121257. [[CrossRef](#)]
31. Krompiec, S.; Filapek, M.; Grudzka-Flak, I.; Slodek, A.; Kula, S.; Malecki, J.G.; Malarz, J.; Szafraniec-Gorol, G.; Penkala, M.; Schab-Balcerzak, E.; et al. Multifaceted Strategy for the Synthesis of Diverse 2,2'-Bithiophene Derivatives. *Molecules* **2015**, *20*, 4565–4593. [[CrossRef](#)] [[PubMed](#)]
32. Kula, S.; Szlapa, A.; Malecki, J.G.; Maroń, A.; Matussek, M.; Schab-Balcerzak, E.; Siwy, M.; Domanski, M.; Sojka, M.; Danikiewicz, W.; et al. Synthesis and photophysical properties of novel multisubstituted benzene and naphthalene derivatives with high 2D- π -conjugation. *Opt. Mater.* **2015**, *47*, 118–128. [[CrossRef](#)]
33. Batsyts, S.; Hübner, E.G.; Namyslo, J.C.; Gjikajb, M.; Schmidt, A. Synthesis and characterization of propeller-shaped mono- to hexacationic quinolinium-substituted benzenes. *Org. Biomol. Chem.* **2019**, *17*, 4102–4114. [[CrossRef](#)] [[PubMed](#)]
34. Kaur, S.; Bhalla, V.; Vij, V.; Kumar, M. Fluorescent aggregates of hetero-oligophenylene derivative as “no quenching” probe for detection of picric acid at femtogram level. *J. Mater. Chem. C* **2014**, *2*, 3936–3941. [[CrossRef](#)]
35. Steel, P.J.; Webb, N.C. Diels–Alder Synthesis of Rigid 60° Angular Bridging Ligands and X-ray Crystal Structures of their Silver Nitrate Complexes. *Eur. J. Inorg. Chem.* **2002**, *9*, 2257–2260. [[CrossRef](#)]
36. Martin, C.J.; Gil, B.; Perera, S.D.; Draper, S.M. Oxidative Bond Formation in Dithienyl Polyphenylenes: Optical and Electrochemical Consequences. *Eur. J. Org. Chem.* **2011**, *2011*, 3491–3499. [[CrossRef](#)]
37. Roberts, D.J.; Nolan, D.; Ó Máille, G.M.; Watson, G.W.; Singh, A.; Ledoux-Rak, I.; Draper, S.M. The synthesis and characterisation of novel ferrocenyl polyphenylenes. *Dalton Trans.* **2012**, *41*, 8850–8860. [[CrossRef](#)] [[PubMed](#)]
38. Frisch, M.J.; Trucks, G.W.; Schlegel, H.B.; Scuseria, G.E.; Robb, M.A.; Cheeseman, J.R.; Scalmani, G.; Barone, V.; Petersson, G.A.; Nakatsuji, H.; et al. *Gaussian 16*; Revision C.01.; Gaussian, Inc.: Wallingford, CT, USA, 2016.
39. Becke, A.D. Density-functional thermochemistry. III. The role of exact Exchange. *J. Chem. Phys.* **1993**, *98*, 5648–5652. [[CrossRef](#)]
40. Yanai, T.; Tew, D.P.; Handy, N.C. A new hybrid exchange-correlation functional using the Coulomb-attenuating method (CAM-B3LYP). *Chem. Phys. Lett.* **2004**, *393*, 51–57. [[CrossRef](#)]
41. Adamo, C.; Barone, V. Toward reliable density functional methods without adjustable parameters: The PBE0 model. *J. Chem. Phys.* **1999**, *110*, 6158–6169. [[CrossRef](#)]
42. Ernzerhof, M.; Scuseria, G.E. Assessment of the Perdew–Burke–Ernzerhof exchange–correlation functional. *J. Chem. Phys.* **1999**, *110*, 5029–5036. [[CrossRef](#)]
43. Rappoport, D.; Furche, F. Property-optimized Gaussian basis sets for molecular response calculations. *J. Chem. Phys.* **2010**, *133*, 134105. [[CrossRef](#)] [[PubMed](#)]
44. Feng, S.; Guo, X.; Zhang, J. An effective strategy for simply varying relative position of two carbazole groups in the thermally activated delayed fluorescence emitters to achieve deep-blue emission. *Spectrochim. Acta A* **2020**, *226*, 117564. [[CrossRef](#)] [[PubMed](#)]
45. Filapek, M.; Matussek, M.; Szlapa, A.; Kula, S.; Pajak, M. The influence of experimental conditions and intermolecular interaction on the band gap determination. Case study of perylene diimide and carbazole-fluorene derivatives. *Electrochim. Acta* **2016**, *216*, 449–456. [[CrossRef](#)]
46. Bujak, P.; Kulszewicz-Bajer, I.; Zagorska, M.; Maurel, V.; Wielgus, I.; Pron, A. Polymers for electronics and spintronics. *Chem. Soc. Rev.* **2013**, *42*, 8895–8999. [[CrossRef](#)] [[PubMed](#)]
47. Krompiec, S.; Filapek, M.; Grudzka, I.; Kula, S.; Slodek, A.; Skorka, Ł.; Danikiewicz, W.; Ledwon, P.; Lapkowski, M. An ambipolar behavior of novel ethynyl-bridged polythiophenes—A comprehensive study. *Synth. Met.* **2013**, *165*, 7–16. [[CrossRef](#)]
48. Turkoglu, G.; Ozturk, T. Electropolymerization, spectroelectrochemistry and electrochromic properties of cross-conjugated and conjugated selenophenothiophenes with thiophene bridge. *Synth. Met.* **2021**, *278*, 116836. [[CrossRef](#)]
49. Li, W.; Chen, L.; Pan, Y.; Yan, S.; Dai, Y.; Liu, J.; Yu, Y.; Qu, X.; Song, Q.; Ouyang, M.; et al. Electrochromic Properties of Polymers/Copolymers via Electrochemical Polymerization Based on Star-Shaped Thiophene Derivatives with Different Central Cores. *J. Electrochem. Soc.* **2017**, *164*, E84. [[CrossRef](#)]
50. Goksu, K.; Hizalan, G.; Udum, Y.A.; Hacıoglu, S.O.; Cevher, S.C.; Toppare, A.L.; Cirpan, A. Syntheses and Characterization of Benzotriazole, Thienopyrroledione, and Benzodithiophene Containing Conjugated Random Terpolymers for Organic Solar Cells. *J. Electrochem. Soc.* **2019**, *166*, H849–H859. [[CrossRef](#)]
51. Yue, H.; Guo, X.; Du, Y.; Zhang, Y.; Du, H.; Zhao, J.; Zhang, J. Synthesis and characterization of donor–acceptor type quinoxaline-based polymers and the corresponding electrochromic devices with satisfactory open circuit memory. *Synth. Met.* **2021**, *271*, 116619. [[CrossRef](#)]
52. Ma, Y.; Du, Y.; Li, C.; Zhang, Y.; Du, H.; Zhao, J.; Zhang, J.; Xie, Y. Synthesis and characterization of D-A type electrochromic polymers based on planar monomers: Cyclopenta[2,1-b,3,4-b']dithiophene and tris (thienothiophene) as electron donors, dike-topyrrolopyrrole as electron acceptor. *Synth. Met.* **2021**, *278*, 116839. [[CrossRef](#)]

53. Filapek, M.; Hellwig, H.; Gancarz, P.; Szłapa-Kula, A. Influence of Various Doping Agents on Organic Semiconductors' Physico-chemical Properties. *J. Electrochem. Soc.* **2021**, *168*, 046508. [[CrossRef](#)]
54. Malacrida, C.; Scapinello, L.; Cirilli, R.; Grecchi, S.; Penoni, A.; Benincori, T.; Ludwigs, S. In Situ Electrochemical Investigations of Inherently Chiral 2,2'-Biindole Architectures with Oligothiophene Terminals. *ChemElectroChem.* **2021**, *8*, 3250–3261. [[CrossRef](#)]
55. Krawczyk, P.; Kula, S.; Seklecka, K.; Łaczkowski, K.Z. Synthesis, electrochemical, optical and biological properties of new carbazole derivatives. *Spectrochim. Acta A* **2022**, *267*, 120497. [[CrossRef](#)] [[PubMed](#)]
56. Zhang, Q.; Zhu, W.; Fang, M.; Yin, F.; Li, C. Synthesis, photophysical and electrochemical properties of two novel carbazole-based dye molecules. *Spectrochim. Acta A* **2015**, *135*, 379. [[CrossRef](#)]

Disclaimer/Publisher's Note: The statements, opinions and data contained in all publications are solely those of the individual author(s) and contributor(s) and not of MDPI and/or the editor(s). MDPI and/or the editor(s) disclaim responsibility for any injury to people or property resulting from any ideas, methods, instructions or products referred to in the content.